Burying Earth's primitive mantle in the slab graveyard

T. D. Jones[1,2], N. Sime[1], P. E. van Keken[1]

[1]Earth and Planets Laboratory, Carnegie Institution for Science, Washington D.C., U.S.A.
[2]Now at Institute of Geophysics and Planetary Physics, University of California San Diego, C.A., U.S.A.

Key Points:

- Subducting oceanic lithopshere entrains primitive mantle as it sinks to the core-mantle boundary
- Dense oceanic crust forms robust thermochemical piles that can trap and preserve primitive material over the age of the Earth
- The mixture of primitive and recycled material may explain the co-existence of these signatures observed in ocean-island basalts
- Numerical models exploiting advection of tracer data yield qualitatively spurious results if the approximation of the Stokes system divergence free constraint is not accurately satisfied pointwise

Corresponding author: T.D. Jones, `t6jones@ucsd.edu`

Abstract

The evolution of mantle composition can be viewed as process of destruction whereby the initial chemical state is overprinted and reworked with time. Analyses of ocean island basalts reveals that some portion of the mantle has survived this process, retaining a chemically 'primitive' signature. A question that remains is how this primitive signature has survived four and half billion years of vigorous convection. We hypothesize that some of Earth's primitive mantle is buried within a slab graveyard at the core-mantle boundary. We explore this possibility using high-resolution finite element models of mantle convection, in which oceanic lithosphere is produced at zones of plate spreading and subducted at zones of plate convergence. Upon subduction, dense oceanic crust sinks to the base of the mantle and gradually accumulates to form broad and robust thermochemical piles. Sinking oceanic crust entrains the surrounding mantle whose composition is predominantly primitive early in the model's evolution. As a result, thermochemical piles are initially supplied with relatively high concentrations of primitive material – summing up to ∼30% their total mass. The dense oceanic crust that dominates the piles resists efficient mixing and preserves the primitive material that it is intermingled with. The significance of this process is shown to be proportional the rate of mantle processing through time and the excess density of oceanic crust at mantle pressures and temperatures. Unlike existing theories for the survival of Earth's primitive mantle, this one does not require the early Earth to have anomalously high density or large scale viscosity contrasts.

Keywords: geodynamics, mantle convection, primitive mantle

Plain Language Summary

When oceanic plates pull apart the mantle melts to form slabs of lithosphere, which are later recycled back into the mantle at subduction zones. This process of melting and subduction destroys the initial chemical signature of the mantle. Geochemical analyses reveal that some portion of the mantle has avoided this process and retained a chemically 'primitive' signature. How this material has survived vigorous convection for ∼4.5 Gyr is an open question. Here we propose that it may be preserved at the base of the mantle in large accumulations of subducted lithosphere. These accumulations are dominated by dense oceanic crust but can comprise up to 30% primitive material. The intermingling of oceanic crust and primitive material may explain why the chemical signatures of both coexist in volcanic eruptions at Earth's surface.

1 Introduction

Nearly all chemical heterogeneity in the mantle is the result of geological processes that have altered its initial composition. The one exception is heterogeneity that exists because some portion of the mantle remains unaltered. This 'primitive material' has been identified by measuring noble gas concentrations of modern mantle derived rocks (Graham et al., 1998; Hilton et al., 1999; Kurz et al., 1982; Saal et al., 2007; Stuart et al., 2003). Its existence is one measure of how (in)efficiently geological processes have changed mantle composition over the past four and half billion years.

The survival of primitive material in the modern mantle is a puzzle for anyone interested in Earth's chemical evolution. Primitive material has been detected in volcanic rocks at geographically widespread locations, suggesting that it is a relatively prevalent mantle reservoir. Examples include ocean island basalts (OIBs) such as Hawaii (Kurz et al., 1982), Samoa (Jackson et al., 2007), Galapagos (Saal et al., 2007) and Iceland (Starkey et al., 2009), and large igneous provinces (LIPs) such as Baffin bay and West Greenland (Jackson et al., 2010). In contrast, a fundamental insight from studies of

mantle mixing is that at present day convective vigor large-scale heterogeneity will be destroyed in less than Earth's lifetime (Hoffman & McKenzie, 1985). Moreover, such estimates can be considered conservative because convective vigor is likely to have been higher in the past due to higher radiogenic heat production.

One possibility is that primitive material possesses physical properties that resist mixing by thermal convection. For example, high density suppresses thermal advection and promotes the segregation of material to the base of the mantle (e.g., Brandenburg et al., 2008; Burke et al., 2008; Christensen & Hofmann, 1994; Garnero & McNamara, 2008; Kellogg et al., 1999; M. Li & McNamara, 2013; Sleep, 1988; Xie & Tackley, 2004). Highly viscous rheologies do not efficiently mix by kinematically driven flows (Manga, 1996) and can preserve material at the core of large convective cells (Ballmer et al., 2017; Becker et al., 1999). Indeed, some combination of both density and viscosity excesses will be most effective in prolonging the lifespan of any mantle reservoir (Deschamps & Tackley, 2008; Y. Li et al., 2014; McNamara & Zhong, 2004).

Such explanations require that early chemical differentiation on Earth endowed some portion of the mantle with distinct rheological and/or thermodynamic properties. Mechanisms that could increase mantle density include core-mantle interaction (e.g., Deschamps et al., 2012), whereby iron-rich material from the core is added to the mantle, and the segregation of iron-rich cumulates during crystallization of a magma ocean (e.g., Labrosse et al., 2007). A crystallizing magma ocean could also produce silica-rich cumulates (e.g., Ballmer et al., 2017), which would be of much higher viscosity than the mantle average. Due to a lack of geological information about the early Earth, it remains uncertain whether such processes actually occurred, let alone caused the requisite change in physical properties that would ensure long-term preservation.

A different type of chemical differentiation process, for which there is ample evidence, is the formation and destruction of oceanic crust. At spreading centers, where oceanic lithosphere is created, the mantle melts to form a thin layer of basaltic crust on top of a thicker layer of harzburgitic residue. At convergent zones, these components are subducted back into the mantle and begin to remix. At upper mantle temperatures and pressures, the basaltic component transforms into higher density lithologies, such as eclogite (Hirose et al., 1999; Irifune & Ringwood, 1993). This gives subducted oceanic crust an excess density with respect to the ambient mantle, which causes it to sink and accumulate at the core-mantle boundary (CMB). This newly formed reservoir is entrained by mantle plumes and returned it to the surface (Chase 1981; Hofmann and White 1980, 1982). Furthermore, large scale convection erodes the reservoir and mixes the former oceanic crust back into the ambient mantle. The dynamics of this process, termed crustal recycling, have been thoroughly explored using geodynamic models and are well understood (Brandenburg & van Keken, 2007; Brandenburg et al., 2008; Christensen & Hofmann, 1994; G. F. Davies, 2002; Jones et al., 2020; Ogawa, 2003; Nakagawa & Tackley, 2004, 2008; Xie & Tackley, 2004).

When the argument for recycling oceanic crust was first made (Chase, 1981; Hofmann & White, 1980, 1982), it was made in the context of a debate about whether the OIB reservoir included a substantial primitive component (e.g., DePaolo & Wasserburg, 1976, 1979). Hofmann et al. (1986) concluded that it did not. Instead they suggested that the trace element characteristics of OIBs could be largely accounted for by a reservoir of ancient oceanic crust. The addition of primitive He by another mechanism, they noted, would be required to explain the high ^{3}He/^{4}He ratios of some OIBs. In favor of this argument is the fact that the formation and subduction of oceanic crust is volumetrically the most significant ongoing differentiation process on Earth and is therefore likely to be a dominant component of the mantle in general. A question that remains is how recycling oceanic crust has influenced the primitive mantle over the course of Earth's history.
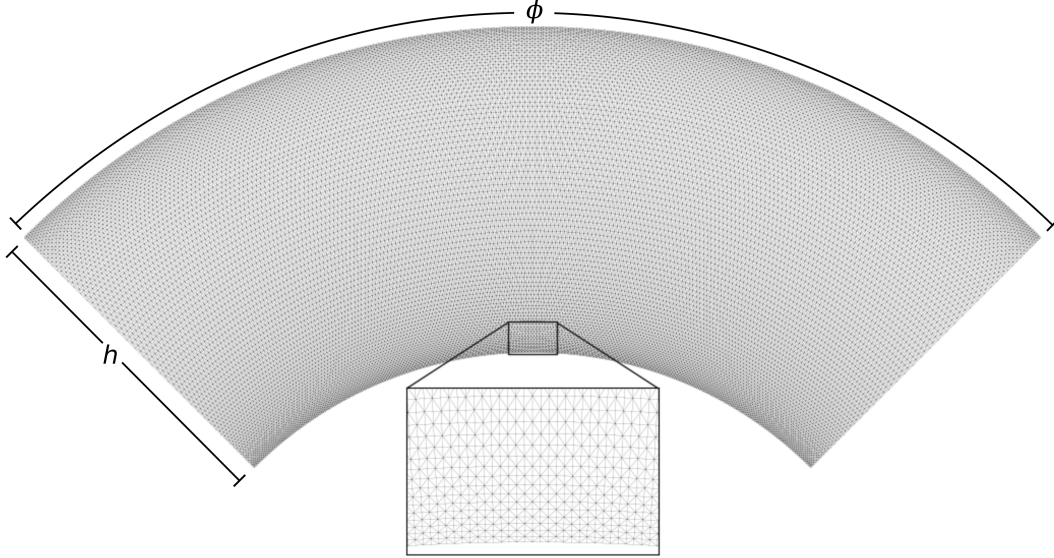
Figure 1: Computational mesh comprising 73 440 cells generated for mantle convection simulations. This represents a resolution of 181 nodal points in the vertical direction. h is the thickness of the mantle, 2885 km, and ϕ is the azimuthal angle in the range 0 to $\frac{\pi}{2}$. To conserve computational cost most of the parameter space is covered using this 'quarter' annulus, while simulations shown in Fig. 7 and Fig. 8 were conducted on the full spherical annulus mesh (see section 2.2 for details).

In this paper we will demonstrate that the mantle's primitive component may owe its survival to the same processes of crustal recycling that explains so well the lithophile element abundances and isotopic compositions of OIBs (e.g., Brandenburg et al., 2008; Chase, 1981; Christensen & Hofmann, 1994; Hofmann & White, 1982). Using geodynamic models of convective mixing, we show that accumulations of oceanic crust at the CMB, which form large thermochemical piles, can contain high concentrations of primitive material (up to ∼30%) and are able to maintain these high concentrations over billions of years of convective mixing. How primitive material concentrates in accumulations of oceanic crust is broadly attributed to entrainment, and in particular entrainment early in Earth's history when the mantle is predominantly primitive in composition. The thermochemical piles observed in our models constitute a reservoir that can account for the coexistence of recycled and primitive signatures in plume derived volcanism. The geochemical significance of such a reservoir is shown to depend upon the rate of mantle processing through time and the excess density of oceanic crust.

2 Methods

2.1 Model Setup and Governing Equations

We model mantle convection in an incompressible Boussinesq fluid at infinite Prandtl number. In non-dimensional form, the governing equations are the conservation of mass

$$\nabla \cdot \boldsymbol{u} = 0 \tag{1}$$

the conservation of momentum

$$-\nabla P + \nabla \cdot \left(\eta \underline{\dot{\epsilon}} \right) = [RaT\alpha(z) - RcC\beta(z)]\hat{\boldsymbol{g}} \tag{2}$$

and the conservation of heat

$$\frac{\partial T}{\partial t} + (\boldsymbol{u} \cdot \nabla)T = \nabla^2 T + Q \tag{3}$$

where $\boldsymbol{u}$ is the velocity vector, P the dynamic pressure, t time, T the temperature, $\hat{\boldsymbol{g}}$ the unit vector in the direction of gravity, α the thermal expansivity, β the generalized chemical compressibility, C the chemical composition, η the non-dimensional dynamic viscosity, and Q is the volumetric internal heating. $\underline{\dot{\epsilon}}$ is the strain-rate tensor

$$\underline{\dot{\epsilon}} = \left(\nabla \boldsymbol{u} + \nabla \boldsymbol{u}^T \right) \tag{4}$$

and Ra is the thermal Rayleigh number

$$Ra = \frac{\rho_0 g \alpha_0 \Delta T h^3}{\kappa_0 \eta_0} \tag{5}$$

where ΔT is the assumed temperature contrast across the mantle and h is the thickness of the mantle. ρ_0, κ_0, α_0, and η_0 are the reference values for density, thermal diffusivity, thermal expansivity, and dynamic viscosity, respectively. Rc is the compositional Rayleigh number

$$Rc = \frac{\rho_0 g \beta_0 \Delta C h^3}{\kappa_0 \eta_0} \tag{6}$$

where ΔC is the chemical contrast between 1, pure basalt, and 0, pure harzburgite (see below). For reference values, see Table 1. The effects of hydrostatic pressure are included by allowing α and β to vary as a function of depth, z

$$\alpha(z) = \frac{d}{1 - e^{-d}} \cdot e^{-dz} \tag{7}$$

$$\beta(z) = \frac{s}{1 - e^{-s}} \cdot e^{-sz} \tag{8}$$

where d and s are constants ln(6) and ln(2), respectively.

We assume a yield stress rheology similar to Nakagawa and Tackley (2015) and Tackley (2000) whereby the viscosity field η is calculated as the harmonic average between a linear part that depends temperature and depth, z, and a nonlinear, plastic part that depends on the strain rate

$$\eta = (\eta_{\text{lin}}^{-1} + \eta_{\text{plast}}^{-1})^{-1}. \tag{9}$$

The linear part is given by

$$\eta_{\text{lin}}(T, z) = \eta(z) \exp\left[\frac{27.631}{T/3.0 + 0.88} \right] \times (5.860\,52 \times 10^{-13}) \tag{10}$$

where $\eta(z)$ is a prefactor

Symbol	Parameter	Reference value	Units
h	Mantle thickness	2885	km
α_0	Thermal expansion coefficient	3×10^{-5}	K^{-1}
ρ_0	Density	4500	kg m^{-3}
κ_0	Thermal diffusivity	10^{-6}	m^2 s^{-1}
ΔT	Temperature contrast	3000	K
Ra	Rayleigh number	10^7	

Table 1: Parameters common to all cases examined and their reference values.

$$\eta(z) = \begin{cases} 1 & z \leq 670\,\text{km}, \\ 30 & z > 670\,\text{km}. \end{cases} \tag{11}$$

The plastic part is given by

$$\eta_{\text{plast}}(z) \;=\; \eta^* + \frac{\sigma_Y + \sigma_b(z)}{\sqrt{\underline{\underline{\dot{\epsilon}}} : \underline{\underline{\dot{\epsilon}}}}} \tag{12}$$

where $\eta^* = 10^{-3}$ is a minimum plastic viscosity threshold, $\sigma_Y = 10^7$ is the constant ductile yield stress and $\sigma_b = 10^7$ is the gradient of brittle yield stress with depth.

2.2 Geometry and Numerical implementation

We simulate mantle mixing in the polar-axially symmetric spherical annulus geometry (Hernlund & Tackley, 2008). We employ two domains: the full annulus Ω and the 'quarter' annulus Ω_{quart} where

$$\Omega = \{(r, \theta, \phi) : (r, \theta, \phi) \in (r_1, r_2) \times \{\frac{\pi}{2}\} \times (0, 2\pi]\}, \tag{13}$$

$$\Omega_{\text{quart}} = \{(r, \theta, \phi) : (r, \theta, \phi) \in (r_1, r_2) \times \{\frac{\pi}{2}\} \times (-\pi/4, \pi/4]\}. \tag{14}$$

Here r, θ and ϕ are the radius, polar angle and azimuthal angle, respectively, and $r_1 = 1.208\,318\,891$ and $r_2 = r_1 + 1$ are the inner core and outer surface radii, respectively. These domains form equatorial slices of the earth. For our finite element computations the full and quarter annuli are subdivided into $293\,760$ and $73\,440$ triangular cells, respectively (Fig. 1). Both meshes have the same spatial resolution with 91 vertices (181 nodal points) in the radial direction.

The velocity and pressure finite element functions are approximated using the standard Taylor–Hood piecewise quadratic and piecewise linear finite element pair. The temperature is also approximated by piecewise quadratic finite elements. Periodic boundary conditions are enforced on the finite element solutions at the azimuthal limits of the domain. At the inner core and outer surface radii the radial component of the velocity is set to zero. In the full annulus at each time step we solve for $1\,332\,163$ and $591\,508$ degrees of freedom in the Stokes and heat equations, respectively. In the quarter annulus with the same number of finite element nodes in the radial direction we solve for $332\,973$ and $147\,696$ degrees of freedom in the Stokes and heat equations, respectively.

To conserve computational cost we run only two simulations on the full mesh, which aids visualization (Fig. 7 and Fig. 8). All other computations were conducted
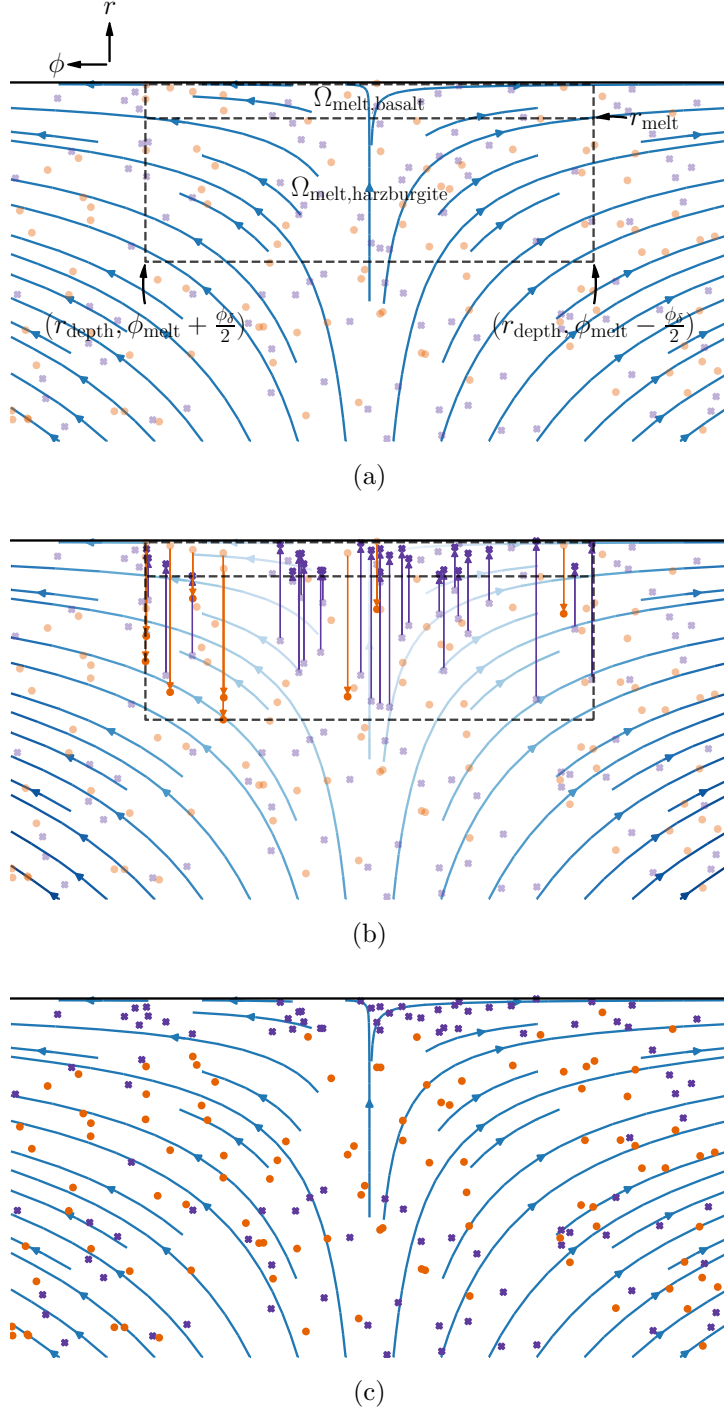
(a)

(b)

(c)

Figure 2: Schematic of the melting process used at the surface of the spherical annulus model, see section 2.2 for details. Here the flow field of an upwelling is represented by the blue streamlines. Harzburgite and basalt particles are shown as purple crosses and orange dots, respectively. (a) The configuration of the flow field satisfies the criterion for generation of a melt zone by eq. (15). (b) Relocating the harzburgite and basalt particles within the melt zone. (c) The same upwelling velocity configuration with the newly melted particles in their new positions.
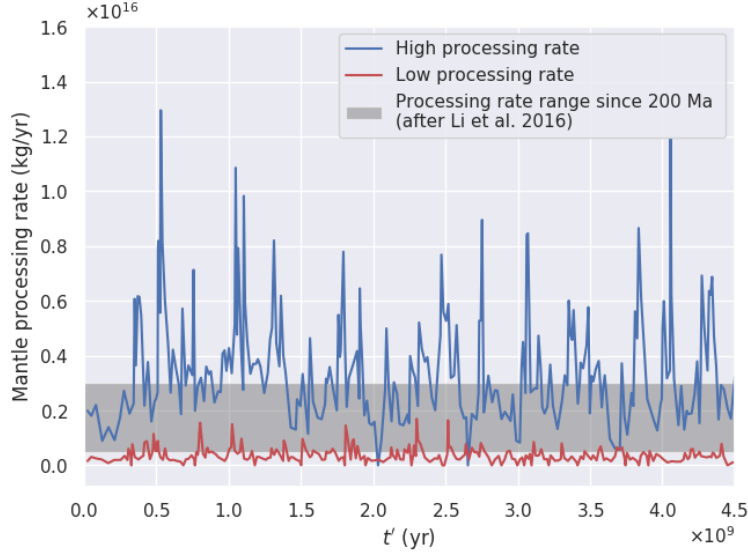
Figure 3: The mass of mantle processing through melt regions as a function of scaled model time (Section 2.4) for the two sets of melting parameters used in this study. For the low processing rate, the melt azimuth arc width is restricted to a maximum of 0.035 or approximately 223 km arc length at the surface. The range given for the past 200 Ma (extended back to t'=0 for comparison with model values) is calculated from the melt production rate of M. Li et al. (2016). The minimum and maximum values assume partial melt fractions of 20% and 10%, respectively, and a crustal density of 3000 kg/km^3.

on the quarter annulus since comparisons with the full annulus yielded the same qualitative results.

We exploit the components of the FEniCS project (Alnæs et al., 2015) to compute numerical approximations of the solutions of eqs. (1) to (3) combined with the particle add-on library LEoPart (Maljaars et al., 2020) to track chemical composition data. FEniCS is particularly useful for simplifying the vector calculus operations in a spherical coordinate system with its automatic generation of high performance code for finite element formulations represented by computational symbolic algebra. To solve the underlying linear system we use the PETSc library (Balay et al., 2019b, 2019a) in combination with MUMPS (Amestoy et al., 2000) for the direct factorization of matrices.

2.3 Mantle compositional and melting

Our approach to modeling mantle composition and melting follows closely that of Brandenburg et al. (2008). The ambient mantle is defined by a simple mechanical mixture of two particle types whose behavior differs upon melting. A mathematical description of the melting process is provided below and is illustrated in Fig. 2. We conceptualize the process in the following way. As packet of fluid rises beneath a melt region for the first time, one half of the particles are moved to the upper 12.5 km of the model domain to form an 'oceanic crust' while the other half are moved to the 87.5 km below the crust to form a lithospheric residue. For simplicity, we refer to these components as 'basalt' and 'harzburgite', and the mixture of both prior to melting as 'lherzolite', despite these being lithological terms with implications that are not accounted for by our model. In accordance with the fact that lithospheric residue is seven times thicker than oceanic crust, harzburgite particles have a volume seven times
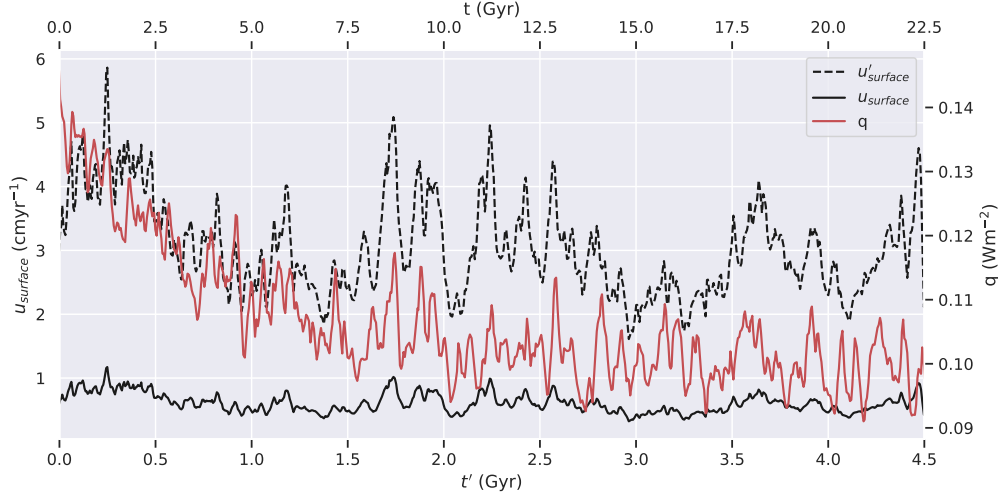
Figure 4: Comparison between output from reference model and measurable quantities: surface heat flux q (red line), dimensional surface velocity u_{surface} (black solid line) and scaled dimensional surface velocity u'_{surface} (black dashed line) resulting from the time scaling provided by eq. (19). q and the scaled dimensional surface velocity of the model are comparable to Earth's q and surface velocity in the poloidal direction.

that of basalt particles. This is cheaper than the alternate approach of increasing the number of harzburgite particles by a factor of seven.

Melt zones are generated in the computational model automatically according to the following procedure:

1. Melt zone locations are determined by measurement of flow spreading at the domain surface exceeding a tolerance criterion

$$\text{spread}(\boldsymbol{u}) := \frac{\partial u_\phi}{\partial \phi} \left(r_2, \frac{\pi}{2}, \phi \right) > \text{TOL}_{\text{spread}}. \tag{15}$$

Here $\text{TOL}_{\text{spread}} = 100$ is the minimum flow spreading tolerance and u_ϕ is the azimuthal component of the velocity field. We further prescribe that this criterion be satisfied over a minimum azimuth arc $\Phi_{\text{spread}} := (\phi_{\text{spread},1}, \phi_{\text{spread},2})$ where $\phi_{\text{spread},2} - \phi_{\text{spread},1} = 0.14\,\text{rad}$ (corresponding to $\sim 892\,\text{km}$ arc length at the surface).

2. Given a satisfied melt zone criterion, the center of melting is positioned at the azimuth argument which maximizes the spread function

$$\phi_{\text{melt}} = \underset{\phi \in \Phi_{\text{spread}}}{\arg\max} \left(\text{spread}(\boldsymbol{u}) \right) \tag{16}$$

and the melt zone spans the azimuthal arc

$$\Phi_{\text{melt}} = \left(\phi_{\text{melt}} - \frac{\phi_\delta}{2}, \phi_{\text{melt}} + \frac{\phi_\delta}{2} \right) \tag{17}$$

where $\phi_\delta = 0.035\,\text{rad}$ is the melt azimuth arc width (approximately $223\,\text{km}$ arc length at the surface).

3. We define the melt zone geometry in terms of the basalt and harzburgite components (Fig. 2a)

$$\Omega_{\text{melt,harzburgite}} = (r_{\text{depth}}, r_{\text{melt}}) \times \Phi_{\text{melt}} \quad \text{and} \quad \Omega_{\text{melt,basalt}} = (r_{\text{melt}}, r_2) \times \Phi_{\text{melt}}. \quad (18)$$

Here $r_{\text{depth}} = r_2 - 0.035$ and $r_{\text{melt}} = r_2 - 0.035/8$ (corresponding to depths of $100\,\text{km}$ and $12.5\,\text{km}$, respectively) are the melt zone depth and melt zone melting radii, respectively.

4. Each basalt particle in $\Omega_{\text{melt,harzburgite}}$ with radial and azimuthal position (r_p, ϕ_p) is relocated to $(\mathcal{U}(r_{\text{melt}}, r_2), \phi_p)$ where $\mathcal{U}(a, b)$ is a random number drawn from a uniform random distribution between a and b. Likewise each harzburgite particle in $\Omega_{\text{melt,basalt}}$ is relocated from (r_p, ϕ_p) to $(\mathcal{U}(r_{\text{depth}}, r_{\text{melt}}), \phi_p)$ (Fig. 2b and Fig. 2c).

2.4 Time scaling, convective vigor and limitations of the yield stress rheology

The vigor of Earth's convection is an important variable in studies of mantle mixing. Since there is no direct measure of velocity through Earth's interior, we rely on surface velocities to define the vigor of convection. However, we have found there to be a trade-off between surface velocities and plate stability when employing the yield-stress formulation defined by eqs. (9) and (10): higher velocities yield lower plate stability and vice versa. Relatively robust plates are maintained at an average surface velocity of $\sim$0.6 cm/yr, approximately one fifth that of Earth's (considering only the poloidal component). To approximate the mantle's mixing history, assuming a constant present-day convective vigor, we run our models for five times the age of the Earth. For comparison with Earth time, post-processing plots are given in terms of a scaled model time, t', based on a model-to-Earth surface velocity ratio:

$$t' = \frac{\bar{u}}{u_0} t \qquad (19)$$

where $\bar{u}$ is the average dimensional surface velocity of the model, u_0 is Earth's average surface velocity in the poloidal direction ($\sim$3 cm/yr) and t is dimensional model time based on a diffusional scaling using κ_0 from Table 1. The dimensional surface velocity, u_{surf}, the scaled dimensional surface velocity, u'_{surf}, and the dimensional surface heat flux, q, for our reference model (no compositional effects) are given in Fig. 4.

Such an approximation cannot capture non-linear effects that scale with convective vigor but is comparable to the approach used by previous studies of similarly low convective vigor (Christensen & Hofmann, 1994; G. F. Davies, 2002; Huang & Davies, 2007; M. Li & McNamara, 2013). Moreover, Brandenburg and van Keken (2007) showed that the scaled time procedure used in Christensen and Hofmann (1994) is reasonable since the geochemical consequences of oceanic crust recycling at low convective vigor could be reproduced in models at full convective vigor.

It appears that the yield-stress rheology is generally used for models that have surface velocities that are substantially below that of the present day Earth. While it is rare that direct evidence of surface velocities is provided, inspection of the top thermal boundary layer in several published models suggest thicknesses generally in excess of 200 km, and sometimes 300 km, implying surface speeds only a fraction of Earth's today (Bocher et al., 2018; Nakagawa et al., 2010, 2015; Tackley, 2000; Trompert & Hansen, 1998; Xie & Tackley, 2004). One solution may be the inclusion of continents, which seems to permit robust plates at Earth-like convective vigor, at least during continental break up (Arnould et al., 2018; Coltice et al., 2013).
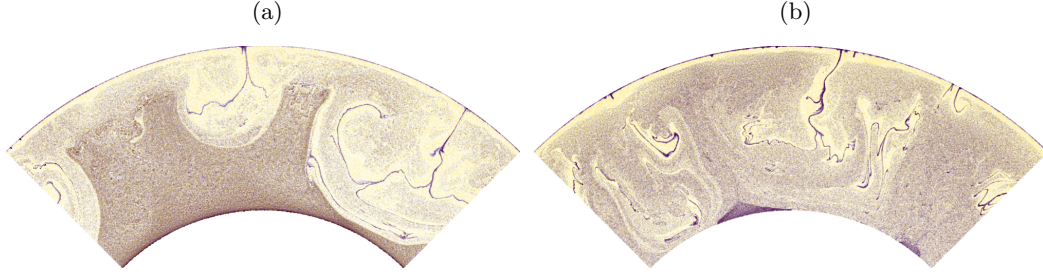
(a) (b)

Figure 5: Example particle fields after $t' \approx 3.5$ Gyr for cases: (a) without the divergence free correction and (b) with the divergence free correction. Basalt particles are blue and harzburgite particles are yellow. Failing to precisely approximate the incompressibility constraint pointwise yields simulations which convey a qualitatively spurious result, including the settling of particles to the base of the model domain. We observe that dense basalt particles accumulate in piles at the CMB only when the divergence free correction is applied.

2.5 Improving the pointwise approximation of a divergence free velocity field

In order to mitigate tracer dispersion (cf. Sime et al., submitted) we use an iterated penalty method to project the velocity approximation onto a solenoidal vector space (see, for example, Morgan & Scott, 2018), which we will refer to as the divergence-free correction. Thus we reduce the pointwise error in our approximation of mass conservation eq. (1) such that $(\int_{\Omega} (\nabla \cdot \boldsymbol{u}_h)^2 \, \mathrm{d}x)^{\frac{1}{2}} < 10^{-7}$ where $\boldsymbol{u}_h$ is the finite element approximation of the velocity. We find the correction is vital to avoid spurious particle behavior, particularly when performing calculations over long time periods relevant for the Earth. To illustrate its impact an example is provided in which two cases are compared: Fig. 5a without the divergence free correction and Fig. 5b with the divergence free correction. The results diverge markedly. For instance, without the correction we observe artificial settling of particles to the base of the model domain (Fig. 5a). In contrast, when the correction is applied dense basalt particles accumulate at the base of the mantle to form piles (Fig. 5b) in a fashion similar to that observed in previous studies (Brandenburg & van Keken, 2007; Brandenburg et al., 2008; Christensen & Hofmann, 1994). This approach of divergence-free correction is demonstrated in more detail in the Supplement by reproduction of one of the models of Christensen and Hofmann (1994) along with open source code in the repository Sime (2020).

3 Results

We vary two parameters across our simulation suite: the rate of mantle processing and the density of oceanic crust. The rates of mantle processing for our models are given in Fig. 3, along with an estimate for the Earth since 200 Ma. To achieve the low processing rate, the melt zone is restricted to a maximum 223 km arc length at the surface. The is no such restriction for the high processing rate. The estimate for Earth is calculated from the range of melt production rates determined by M. Li et al. (2016) assuming the average crustal density to be 3000 kg/m^3 and the fraction of partial melting to be between 10–20%. The excess density of oceanic crust is defined as $\delta \ln \rho = (\rho_B - \rho_L)/\rho_L$, where ρ_B and ρ_L are the density of basalt and lherzolite, respectively. $\delta \ln \rho$ is set to 0%, 4% and 6%. This choice falls within the range of experimentally predicted values for oceanic crust in the lower mantle (Aoki & Takahashi, 2004; Hirose
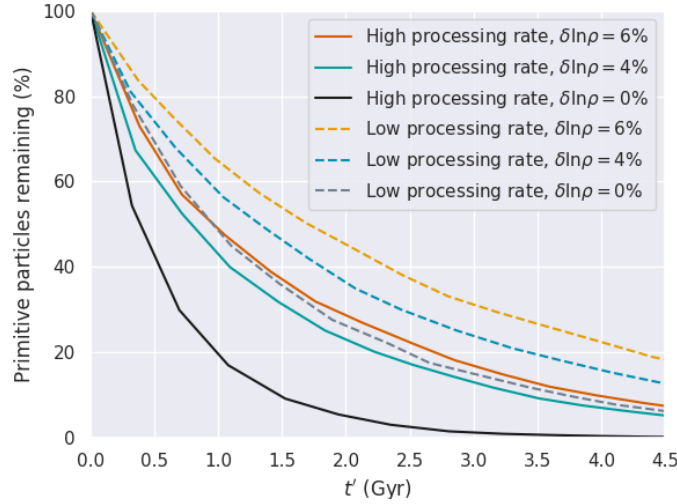
Figure 6: The number of primitive (yet to pass through a melt zone) particles as a function of scaled model time (Section 2.4) for all models. The proportion of primitive particles decreases exponentially with time. The rate of exponential decay is dependent on both the melt flux and the excess density of oceanic crust. A small portion survive to the end of simulation time in all cases.

et al., 1999, 2005; Ricolleau et al., 2010; Ringwood & Irifune, 1988; Ringwood, 1990; Tsuchiya, 2011) and follows from previous studies showing the accumulation of oceanic crust to be substantial when $\delta\ln\rho \geq 3\%$ (Brandenburg et al., 2008; Jones et al., 2020).

To examine the preservation of the primitive mantle we track the melting history of the particles. Each particle falls into one of two categories, either primitive or processed. At $t' = 0$, all particles are considered primitive. During simulation, should a primitive particle pass through a melt region, that particle becomes 'processed'. Particles that are yet to melt retain their original primitive designation. Let t'_x be the current scaled model time and $t'_{n,\mathrm{melt}}$ be the scaled model time since the nth particle last passed through a melt zone. We define the nth particle's age

$$\lambda_n = t'_x - t'_{n,\mathrm{melt}} \tag{20}$$

3.1 Decline of the primitive mantle: effects of melt flux and excess density of oceanic crust

Regardless of the chosen melt flux or excess density, the proportion of primitive particles in the mantle exponentially decays as a function of time (Fig. 6). After $t' = 4.5$ Gyr, a majority of the mantle has experienced melting. The proportion of primitive particles that survive increases with the excess density of oceanic crust and decreases with the rate of mantle processing (Fig. 6).

To quantify the effects of compositional buoyancy we first examine a reference case, where oceanic crust has no excess density and thus convection is driven by thermal buoyancy alone. The final temperature and composition state are given in Fig. 7. The formation of oceanic lithosphere and its subsequent remixing leads to a marble cake pattern and the mantle becoming dominated by recycled material.
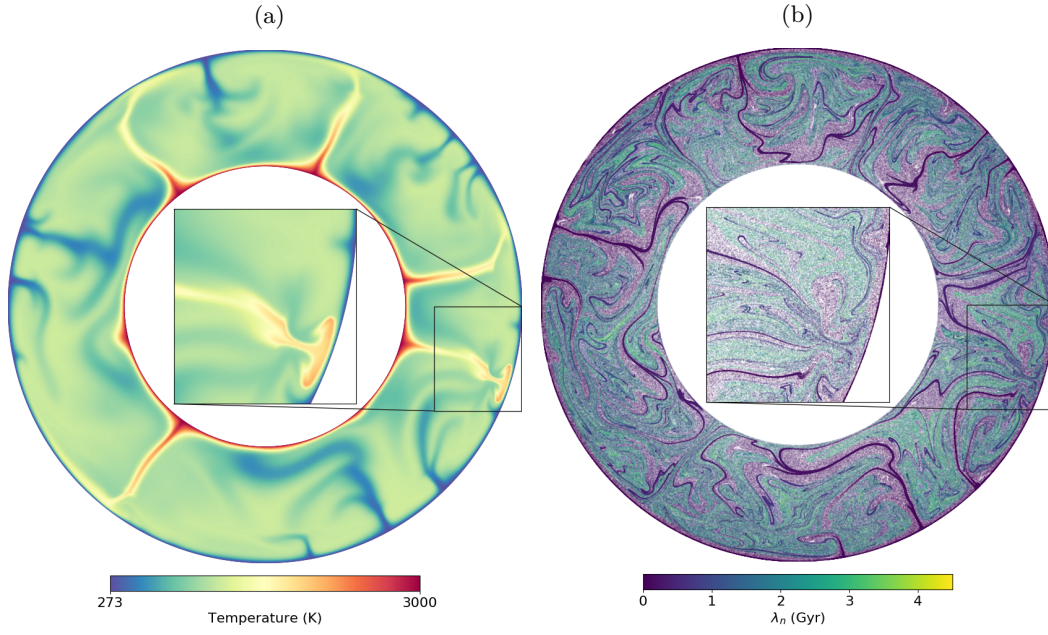
Figure 7: (a) Temperature field and (b) particle field for case with $\delta \ln \rho = 0\%$ and high melt flux. Colors in (b) correspond to the particle age, λ_n, defined as the duration of scaled time since a particle last past through a melt zone (eq. (20)). As oceanic crust does not accumulate at the CMB, broad-scale compositional structure is absent. Inset highlights fluid dynamic features of plume head and thinning of the lithosphere captured by the high resolution simulation.
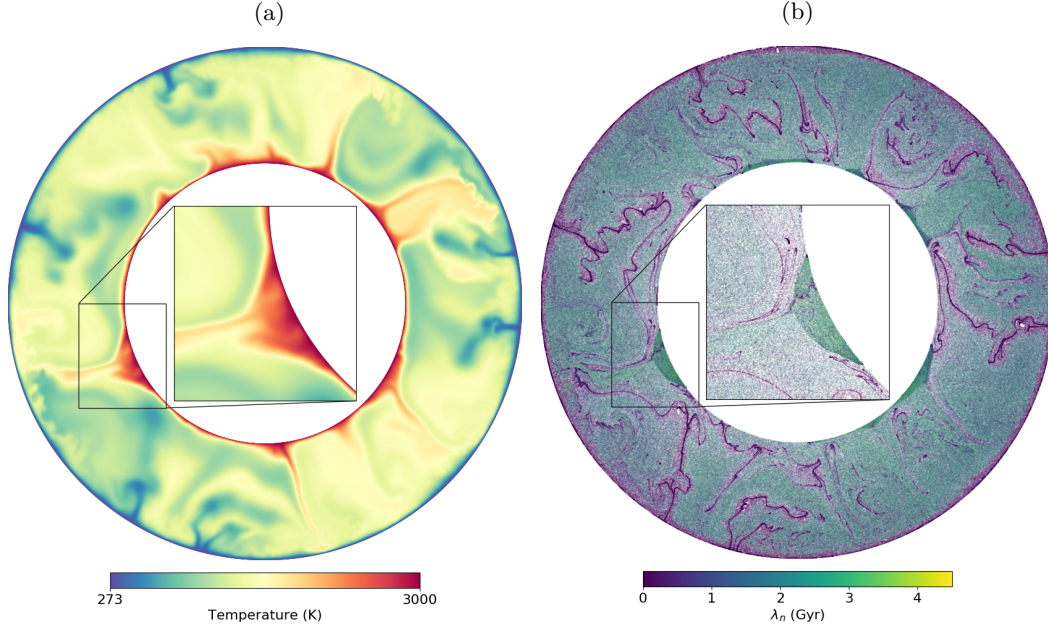
Figure 8: (a) Temperature field and (b) particle field for case with $\delta\ln\rho = 6\%$ and high melt flux. Colors in (b) correspond to the particle age, λ_n, defined as the duration of scaled time since a particle last past through a melt zone (eq. (20)). The excess density of oceanic crust promotes its accumulation at the core-mantle boundary and the formation of thermochemical piles, which consequently preserves primitive material. Inset highlights internal structure of thermochemical piles captured by the high resolution simulation.

Introducing an excess crustal density leads to important changes in the mantle's compositional structure and initiates a process of crustal recycling. The density contrast causes oceanic crust to segregate from its harzburgite residue and accumulate at the base of the mantle to form broad thermochemical piles (Fig. 8). The cycle completes once material inside the piles is entrained by upwellings and returned to the surface to form new oceanic crust.

Significantly, models with an excess crustal density preserve more primitive material than the purely thermal reference case (Fig. 6). The higher the excess density, the greater the number of surviving primitive particles. We explore why this is the case in the next section.

3.2 Primitive mantle and ancient oceanic crust in thermochemical piles

Histograms of particle age (eq. (20)) reveal that the ambient mantle and thermochemical piles are distinct geochemical reservoirs (Fig. 9). Thermochemical piles are quantitatively defined by grid cells that have greater than 30% oceanic crust, and are part of a vertically continuous column starting at the CMB. The age distribution for oceanic crust (basalt particle) in the ambient mantle is skewed towards younger ages whereas the age distribution of oceanic crust in thermochemical piles is more random, often with young and old ages equally well represented. The exception to this trend being the case with a high mantle processing rate and $\delta\ln\rho$ of 4% (Fig. 9g), where younger oceanic crust dominates the distribution. Ages younger than the time it takes oceanic crust to reach the CMB are naturally absent from thermochemical piles.
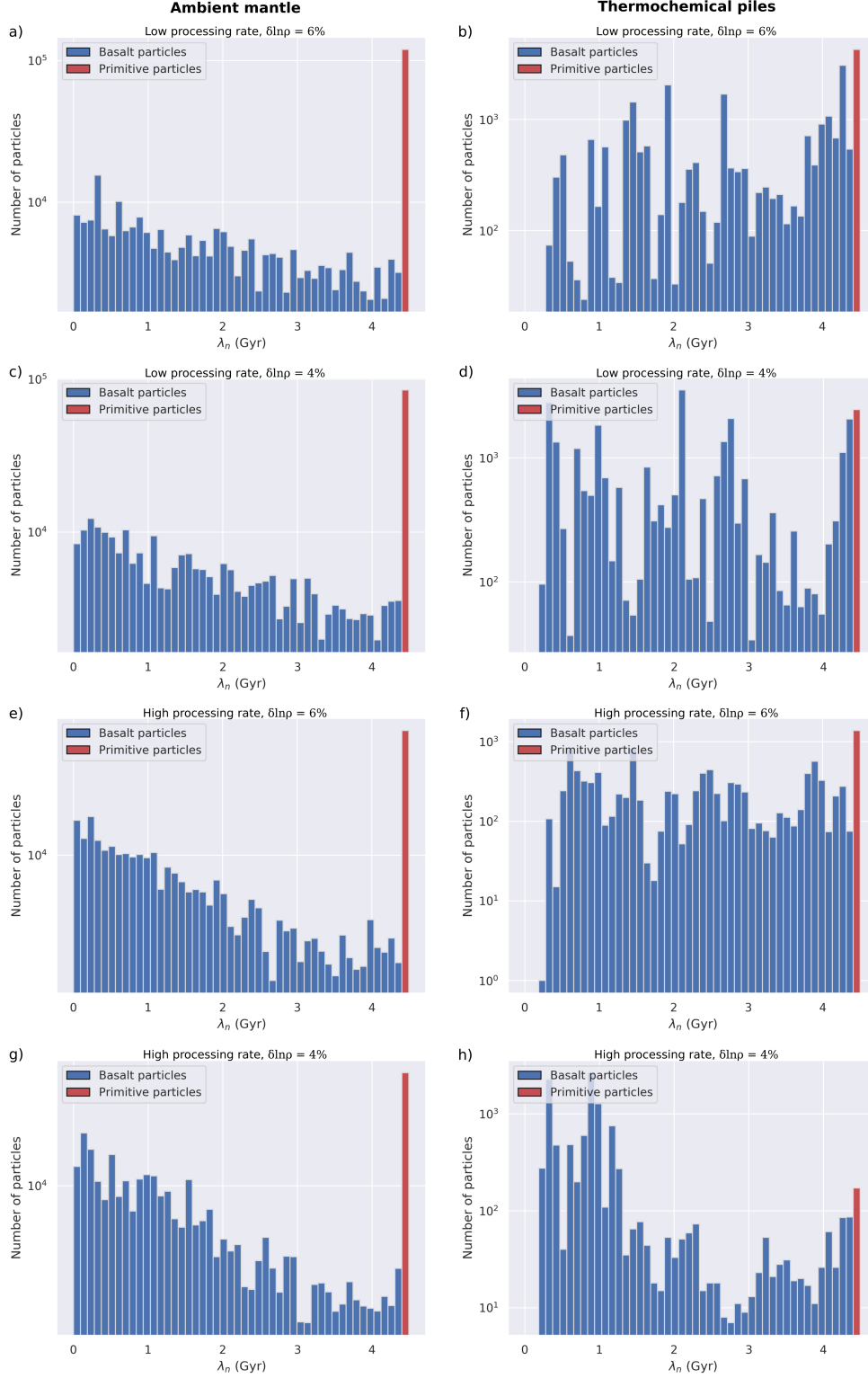
Figure 9: Histograms of particle age, λ_n, for basalt particles (blue) and primitive particles (red) in the ambient mantle (left column) and thermochemical piles (right column). Thermochemical piles are quantitatively defined by grid cells that have greater than 30% oceanic crust and are part of a vertically continuous column starting at the CMB. Each row contains data from a single simulation. Processing rate and $\delta \ln \rho$ is given above each plot. Primitive particles, which have never melted, are plotted in the 4.5 Gyr age bin. In the ambient mantle the distribution of oceanic crust ages is skewed toward younger ages, while older ages are generally equally well represented in thermochemical piles, with the exception of (h) where younger material has recently been added to a thermochemical pile.
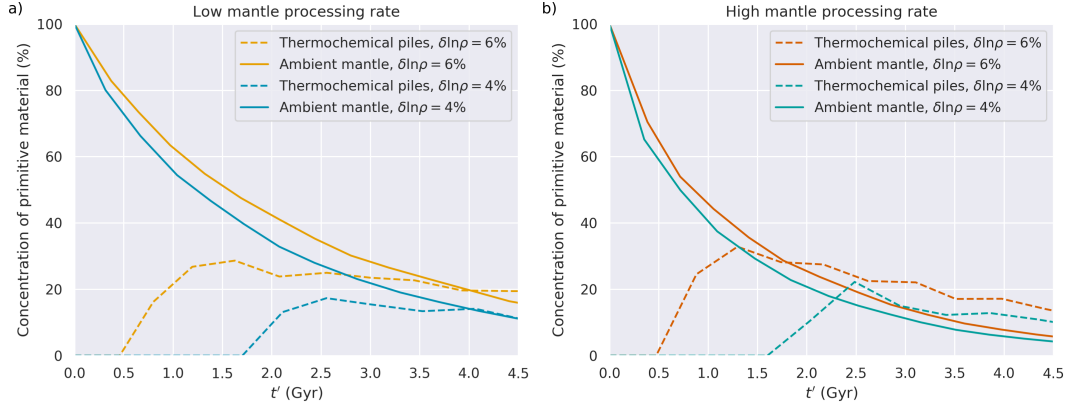
Figure 10: The concentration, by mass, of primitive particles in the ambient mantle and thermochemical piles as a function of scaled model time (see Section 2.4) for (a) low mantle processing and (b) high mantle processing. Thermochemical piles are quantitatively defined by grid cells that have greater than 30% oceanic crust, and are part of a vertically continuous column starting at the CMB. The concentration decays exponentially in the ambient mantle but only linearly in thermochemical piles. By the end of the simulations, thermochemical piles have a higher concentration of primitive material than the ambient mantle. The concentration of primitive material is set to zero when the mass of thermochemical piles is <1% of the mantle total.)

Primitive particles, that is those yet to melt, are plotted in the 4.5 Gyr age bin. In all cases the number of primitive particles that remain is greater than any other age bin of the ambient mantle distribution. The same is true for thermochemical piles when the excess density of oceanic crust is high ($\delta\ln\rho = 6\%$), irrespective of the mantle processing rate.

What is important to the detection of primitive material in the mantle is its relative abundance. In cases where the mantle processing rate is low and $\delta\ln\rho = 6\%$ (Fig. 10a), the concentration of primitive material in thermochemical piles, by mass, is around 20% by $t' = 4.5$ Gyr and just a few percent less in the ambient mantle. Lowering $\delta\ln\rho$ to 4% drops the concentration of primitive material to 16% in thermochemical piles and about the same in the ambient mantle.

In cases where the mantle processing rate is high, the difference in primitive material concentration between thermochemical piles and the ambient mantle increases. When $\delta\ln\rho = 6\%$, (Fig. 10b) primitive material constitutes 15% of thermochemical piles and just 5% of the ambient mantle. Lowering $\delta\ln\rho$ to 4%, primitive material constitutes 11% of thermochemical piles and just 4% of the ambient mantle.

Our results indicate that the dominant reservoir for primitive material in the mantle is time dependent. While both reservoirs lose primitive material with time, the decline in concentration is exponential for the ambient mantle but only linear for thermochemical piles. For the high mantle processing rate, the concentration of primitive material in thermochemical piles does not exceed the ambient mantle until after the first ∼1.8 Gyr (Fig. 10b). And not until after the first ∼2.3 Gyr for the low mantle processing rate (Fig. 10a).

4 Discussion

The distribution of primitive material in the modern mantle has implications for Earth's chemical and dynamical evolution. We suggest primitive material may reside,

and be preserved within, thermochemical piles that form by the accumulation of dense oceanic crust at the CMB. Under this hypothesis, crustal recycling plays a critical role in the distribution of primitive material throughout the mantle and may explain the observation that many OIBs contain both primitive and recycled material. The significance of this process ultimately depends upon the rate of mantle processing through time and the excess density of oceanic crust.

There are two aspects to the relatively high concentration of primitive material in thermochemical piles that must be accounted for. The first is how primitive material is incorporated into thermochemical piles in the first place. The second is the longevity of primitive material in the piles despite efficient mixing of the ambient mantle. The latter is the simplest to explain: the excess density of oceanic crust provides negative buoyancy to thermochemical piles that allows them resist convective mixing and retain a higher concentration of both primitive material and ancient oceanic crust. This becomes clear when we consider that the concentration of primitive material in thermochemical piles is proportional to the density of oceanic crust (Fig. 10).

The former has several plausible mechanisms for which we only highlight the potential of here. (i) Viscous coupling causes cold subducting lithosphere to entrain the surrounding mantle as it sinks to the CMB. (ii) As slabs warm, deform and fold, the surrounding mantle may become trapped between folds. (iii) Lastly, subducting lithosphere arriving at the CMB may trap the mantle beneath it. Each mechanism will most effectively capture primitive material during the early stages of Earth's history when most of the mantle is yet to experience melting. The fluid dynamics of these processes is investigated by Griffiths and Turner (1988).

Although our hypothesis can explain the survival of primitive material, whether it can account for the primitive signature found in OIBs is another question. Primitive mantle is identifiable by its noble gas content – high ^{3}He/^{4}He, for example – raising an additional problem: the thermochemical piles in our models are dominated by recycled material, which has been outgassed and thus contains virtually no ^{3}He. This effectively reverses the scenario proposed by Li et al. (2014), who suggest that recycled crust is a minor component in a sea of primitive material. The question for our model is how a primitive noble gas signature remains detectable in OIBs. Given the compositional variation within thermochemical piles, we speculate that mantle plumes can intermittently entrain primitive material without a large recycled component. This would explain why many OIBs exhibit high ^{3}He/^{4}He (e.g. Konrad et al., 2018; Kurz et al., 1987) alongside distinctly recycled signatures (Hart et al., 1992; Hofmann, 1997; Zindler & Hart, 1986), including some of the highest ^{3}He/^{4}He locations (Brown & Lesher, 2014; Hauri, 1996; Pietruszka et al., 2013; Shorttle & Maclennan, 2011; Sobolev et al., 2005).

Unlike previous explanations for the survival of a primitive reservoir, ours does not require early chemical differentiation of the mantle to cause large-scale variations in physical properties. But, as many authors have argued (Ballmer et al., 2016; Burke et al., 2008; Garnero & McNamara, 2008; M. Li & McNamara, 2013; McNamara & Zhong, 2005), early chemical differentiation may be required to explain large-scale variations in Earth's seismic structure. Due to their unique seismic characteristics, large low-shear velocity provinces (LLSVPs) have widely been interpreted as domains of distinct composition. If this interpretation is correct, an early formed chemical reservoir could account for their existence. However, at present, one cannot reliably infer the composition of LLSVPs from their seismic characteristics (D. Davies et al., 2012, 2015; Koelemeijer et al., 2018; Lau et al., 2017; Schuberth et al., 2009). In fact, Jones et al. (2020) demonstrate that the size and strength of their seismic signature are well explained by the same accumulations of oceanic crust that we argue has preserved Earth's primitive material throughout history. Thus, a more parsimonious

view of mantle evolution may not require large-scale physical properties variations in the early Earth.

In contrast to our findings, M. Li and McNamara (2013) conclude that the accumulation of oceanic crust at the base of the mantle is not an important dynamic process. Their results show that the amount of accumulation at the CMB may be negligible and thus unable to produce broad thermochemical structures. In their models, oceanic crust is recycled back to the surface in mantle plumes "...at a rate equal to or greater than it is accumulated [at the CMB]", despite having a relatively high excess density (up to 4.5%). This point of difference may be explained by a difference of geometry and rheology. M. Li and McNamara's (2013) use of a rectangular Cartesian geometry inhibits the accumulation of oceanic crust at the CMB in two important ways. Both are associated with the exaggerated core to surface ratio (1:1) of their domain. First, this kind of geometry leads to excessive internal temperatures when compared to the Earth and must be corrected for by reducing the internal heating rate (O'Farrell & Lowman, 2010; O'Farrell et al., 2013) – a point M. Li and McNamara (2013) make themselves and indeed correct for by setting internal heat production to zero. However, this correction introduces its own artifact. For internal heating acts to increase the excess temperature of subducting lithosphere (Bercovici et al., 1989) and reduce that of mantle plumes (Bunge, 2005). This skews the competition between accumulating oceanic crust and its entrainment by mantle plumes towards the latter. Secondly, any oceanic crust that reaches the CMB in a rectangular geometry is naturally spread over a distance equal to that of the surface. In more Earth-like geometries, where the core is a fraction of the surface area, oceanic crust is more likely to accumulate and be swept together by broader convective cells (e.g. Brandenburg et al., 2008; Mulyukova et al., 2015; Nakagawa and Tackley, 2010; Yan et al., 2020). Finally, M. Li and McNamara (2013) use a viscosity that is higher overall, less temperature dependent than is adopted here, and not stress-dependent. The first two rheological aspects will contribute to the relatively small amount of accumulated crust at the base of their models, since lower viscosity enhances the segregation of dense material (Nakagawa & Tackley, 2014). The last rheological aspect will cause the top boundary layer to be sluggish due to the high viscosity there and will lead to low rates of recycling of thin oceanic crust in the first place.

There are several parameters that have a particularly strong influence on mantle mixing that are not explored in this study: (i) variations in rheology, (ii) phase transitions and (iii) Earth's 3D spherical geometry. (i) The measurable effects of Earth's convective vigor are limited to the velocity of tectonic plate motions and surface heat flow. We scale time to account for the low convective vigor of our models. However, further uncertainty is introduced through rheological parameters, which could be reasonably adjusted to permit a wider range of estimates for the vigor of convection and, thus, preservation of primitive mantle domains. (ii) Phase transitions may play an important role in the distribution of recycled crust throughout the mantle. As previous studies have shown (Ballmer et al., 2015; Nakagawa et al., 2010), the phase transition at 660 km, depending on its thermodynamic properties, could lead to the accumulation of basaltic crust across the mantle transition zone. The effects of phase changes and that of compressibility in general will be explored in separate work. (iii) Finally, while the 'spherical annulus' of Hernlund and Tackley (2008) retains spherical scaling between CMB radius and surface radius it lacks the toroidal component inherent to mantle convection in a sphere. For the time being, however, 2D calculations remain attractive due to the required high resolution for these thermochemical convection simulations and time evolution over the age of the Earth.

5 Conclusions

We use thermochemcial convection models to examine where and how primitive material is distributed throughout the mantle. We find that if subducted oceanic crust is sufficiently dense it will entrain and trap primitive material as it accumulates at the CMB. Thermochemical piles formed by this process comprise up to 30% primitive material and are robust enough to preserve primitive material in higher concentrations than the ambient mantle. Finally, the intermingling of primitive and recycled material in thermochemical piles is one possible explanation for the observation that primitive and recycled material coexist in many OIBs.

6 Acknowledgements

Acronyms

CMB core-mantle boundary
OIB ocean island basalt
LIP large igneous province

References

Alnæs, M. S., Blechta, J., Hake, J., Johansson, A., Kehlet, B., Logg, A., ... Wells, G. N. (2015). The FEniCS Project Version 1.5. *Archive of Numerical Software*, *3*(100).

Amestoy, P. R., Duff, I. S., & L'Excellent, J.-Y. (2000). Multifrontal parallel distributed symmetric and unsymmetric solvers. *Computer methods in applied mechanics and engineering*, *184*, 501-520.

Aoki, I., & Takahashi, E. (2004). Density of MORB eclogite in the upper mantle. *Physics of the Earth and Planetary Interiors*, *143*, 129–143.

Arnould, M., Coltice, N., Flament, N., Seigneur, V., & Müller, R. (2018). On the scales of dynamic topography in whole-mantle convection models. *Geochemistry, Geophysics, Geosystems*, *19*, 3140-3163.

Balay, S., Abhyankar, S., Adams, M. F., Brown, J., Brune, P., Buschelman, K., ... Zhang, H. (2019a). *PETSc users manual* (Tech. Rep. No. ANL-95/11 - Revision 3.12). Argonne National Laboratory. https://www.mcs.anl.gov/petsc.

Balay, S., Abhyankar, S., Adams, M. F., Brown, J., Brune, P., Buschelman, K., ... Zhang, H. (2019b). *PETSc Web page.* https://www.mcs.anl.gov/petsc.

Ballmer, M., Houser, C., Hernlund, J., Wentzcovitch, R., & Hirose, K. (2017). Persistence of strong silica-enriched domains in the Earth's lower mantle. *Nature Geoscience*, *10*(3), 236–240.

Ballmer, M., Schmerr, N., T. Nakagawa, T., & Ritsema, J. (2015). Compositional mantle layering revealed by slab stagnation at ∼1000 km depth. *Science Advances*, *1*(11), e1500815.

Ballmer, M., Schumacher, L., Lekic, V., Thomas, C., & Ito, G. (2016). Compositional layering within the large low shear-wave velocity provinces in the lower mantle.

Geochemistry, Geophysics, Geosystems, *17*(12), 5056–5077.

Becker, T., Kellogg, J., & O'Connell, R. (1999). Thermal constraints on the survival of primitive blobs in the lower mantle. *Earth and Planetary Science Letters*, *171*(3), 351–365.

Bercovici, D., Schubert, G., & Glatzmaier, G. (1989). Influence of heating mode on three-dimensional mantle convection. *Geophysical Research Letters*, *16*(7), 617–620.

Bocher, M., Fournier, A., & Coltice, N. (2018). Ensemble Kalman filter for the reconstruction of the earth's mantle circulation. *Nonlinear Processes in Geophysics*, *25*(1), 99–123.

Brandenburg, J. P., Hauri, E. H., van Keken, P. E., & Ballentine, C. J. (2008). A multiple-system study of the geochemical evolution of the mantle with force-balanced plates and thermochemical effects. *Earth and Planetary Science Letters*, *276*(1-2), 1–13.

Brandenburg, J. P., & van Keken, P. E. (2007). Deep storage of oceanic crust in a vigorously convecting mantle. *Journal of Geophysical Research*, *112*, B06403.

Brown, E. L., & Lesher, C. E. (2014). North Atlantic magmatism controlled by temperature, mantle composition and buoyancy. *Nature Geoscience*, *7*(11), 820–824.

Bunge, H.-P. (2005). Low plume excess temperature and high core heat flux inferred from non-adiabatic geotherms in internally heated mantle circulation models. *Physics of the Earth and Planetary Interiors*, *153*(1-3), 3–10.

Burke, K., Steinberger, B., Torsvik, T., & Smethurst, M. (2008). Plume generation zones at the margins of large low shear velocity provinces on the core-mantle boundary. *Earth and Planetary Science Letters*, *265*(1-2), 49–60.

Chase, C. G. (1981). Oceanic island Pb: two-stage histories and mantle evolution. *Earth and Planetary Science Letters*, *52*(2), 277–284.

Christensen, U. R., & Hofmann, A. W. (1994). Segregation of subducted oceanic crust in the mantle. *Journal of Geophysical Research*, *99*, 19867–19884.

Coltice, N., Seton, M., Rolf, T., Müller, R., & Tackley, P. (2013). Convergence of tectonic reconstructions and mantle convection models for significant fluctuations in seafloor spreading. *Earth and Planetary Science Letters*, *383*, 92–100.

Davies, D., Goes, S., Davies, J., Schuberth, B., Bunge, H., & Ritsema, J. (2012). Reconciling dynamic and seismic models of Earth's lower mantle: the dominant role of thermal heterogeneity. *Earth and Planetary Science Letters*, *353*, 253–269.

Davies, D., Goes, S., & Lau, H. (2015). Thermally dominated deep mantle LLSVPs: a review. In A. Khan & F. Deschamps (Eds.), *The Earth's heterogeneous mantle* (pp. 441–477). Switzerland: Springer.

Davies, G. F. (2002). Stirring geochemistry in mantle convection models with stiff plates and slabs. *Geochimica et Cosmochimica Acta*, *66*, 3125–3142.

DePaolo, D., & Wasserburg, G. (1976). Inferences about magma sources and mantle structure from variations of $^{143}Nd/^{144}Nd$. *Geophysical Research Letters*, *3*(12), 743–746.

DePaolo, D., & Wasserburg, G. (1979). Petrogenetic mixing models and Nd-Sr isotopic patterns. *Geochimica et Cosmochimica Acta*, *43*(4), 615–627.

Deschamps, F., Cobden, L., & Tackley, P. J. (2012). The primitive nature of large low shear-wave velocity provinces. *Earth and Planetary Science Letters*, *349*, 198–208.

Deschamps, F., & Tackley, P. J. (2008). Searching for models of thermo-chemical convection that explain probabilistic tomography: I. Principles and influence of rheological parameters. *Physics of the Earth and Planetary Interiors*, *171*(1-4), 357–373.

Garnero, E., & McNamara, A. (2008). Structure and dynamics of Earth's lower mantle. *Science*, *320*, 626–628.

Graham, D. W., Larsen, L., Hanan, B., Storey, M., Pedersen, A., & Lupton, J. (1998). Helium isotope composition of the early Iceland mantle plume inferred from the Tertiary picrites of West Greenland. *Earth and Planetary Science Letters*, *160*(3-4),

241–255.

Griffiths, R., & Turner, J. (1988). Viscous entrainment by sinking plumes. *Earth and Planetary Science Letters*, *90*(4), 467–477.

Hart, S. R., Hauri, E. H., Oschmann, L. A., & Whitehead, J. A. (1992). Mantle plumes and entrainment: isotopic evidence. *Science*, *256*, 517–520. doi: 10.1126/science.256.5056.517

Hauri, E. H. (1996). Major-element variability in the Hawaiian mantle plume. *Nature*, *382*, 415–419.

Hernlund, J., & Tackley, P. (2008). Modeling mantle convection in the spherical annulus. *Physics of the Earth and Planetary Interiors*, *171*(1-4), 48–54.

Hilton, D. R., Grönvold, K., Macpherson, C. G., & Castillo, P. R. (1999). Extreme ^{3}He/^{4}He ratios in northwest Iceland: constraining the common component in mantle plumes. *Earth and Planetary Science Letters*, *173*(1-2), 53–60.

Hirose, K., Fei, Y., Y., M., & Mao, H.-K. (1999). The fate of subducted basaltic crust in the Earth's lower mantle. *Nature*, *397*, 53–56.

Hirose, K., Takafuji, N., Sata, N., & Ohishi, Y. (2005). Phase transition and density of subducted MORB crust in the lower mantle. *Earth and Planetary Science Letters*, *237*, 239–251.

Hoffman, N., & McKenzie, D. (1985). The destruction of geochemical heterogeneities by differential fluid motions during mantle convection. *Geophysical Journal International*, *82*(2), 163–206.

Hofmann, A. W. (1997). Mantle geochemistry: the message from oceanic volcanism. *Nature*, *385*, 219–229. doi: 10.1038/385219a0

Hofmann, A. W., Jochum, K., Seufert, M., & White, W. M. (1986). Nb and Pb in oceanic basalts: new constraints on mantle evolution. *Earth and Planetary Science Letters*, *79*(1-2), 33–45.

Hofmann, A. W., & White, W. M. (1980). The role of subducted oceanic crust in mantle evolution. In *Carnegie Institution of Washington Yearbook* (Vol. 79, pp. 477–483).

Hofmann, A. W., & White, W. M. (1982). Mantle plumes from ancient oceanic crust. *Earth and Planetary Science Letters*, *57*, 421–436.

Huang, J., & Davies, G. F. (2007). Geochemical processing in a three-dimensional regional spherical shell model of mantle convection. *Geochemistry, Geophysics, Geosystems*, *8*, Q11006.

Irifune, T., & Ringwood, A. (1993). Phase transformations in subducted oceanic crust and buoyancy relationships at depths of 600–800 km in the mantle. *Earth and Planetary Science Letters*, *117*(1-2), 101–110.

Jackson, M. G., Carlson, R. W., Kurz, M. D., Kempton, P. D., Francis, D., & Blusztajn, J. (2010). Evidence for the survival of the oldest terrestrial mantle reservoir. *Nature*, *466*(7308), 853–856.

Jackson, M. G., Kurz, M. D., Hart, S. R., & Workman, R. K. (2007). New Samoan lavas from Ofu Island reveal a hemispherically heterogeneous high ^{3}He/^{4}He mantle. *Earth and Planetary Science Letters*, *264*(3-4), 360–374.

Jones, T. D., Maguire, R. R., van Keken, P. E., Ritsema, J., & Koelemeijer, P. (2020). Subducted oceanic crust as the origin of seismically slow lower-mantle structures. *Progress in Earth and Planetary Science*, *7*, 17. doi: 10.31223/osf.io/k98p7

Kellogg, L., Hager, B., & van der Hilst, R. (1999). Compositional stratification in the deep mantle. *Science*, *283*, 1881–1884.

Koelemeijer, P., Schuberth, B. S., Davies, D. R., Deuss, A., & Ritsema, J. (2018). Constraints on the presence of post-perovskite in Earth's lowermost mantle from tomographic-geodynamic model comparisons. *Earth and Planetary Science Letters*, *494*, 226–238.

Konrad, K., Graham, D. W., Kent, A. J., & Koppers, A. A. (2018). Spatial and temporal variability in Marquesas Islands volcanism revealed by ^{3}He/^{4}He and the composition of olivine-hosted melt inclusions. *Chemical Geology*, *477*, 161–176.

Kurz, M., Garcia, M., Frey, F., & O'brien, P. (1987). Temporal helium isotopic variations

within Hawaiian volcanoes: basalts from Mauna Loa and Haleakala. *Geochimica et Cosmochimica Acta*, *51*(11), 2905–2914.

Kurz, M., Jenkins, W., & Hart, S. (1982). Helium isotopic systematics of oceanic islands and mantle heterogeneity. *Nature*, *297*(5861), 43–47.

Labrosse, S., Hernlund, J., & Coltice, N. (2007). A crystallizing dense magma ocean at the base of the Earth's mantle. *Nature*, *450*, 866–869.

Lau, H. C. P., Mitrovica, J. X., Davis, J. L., Tromp, J., Yang, H.-Y., & Al-Attar, D. (2017). Tidal tomography constrains Earth's deep-mantle buoyancy. *Nature*, *551*, 321-326.

Li, M., Black, B., Zhong, S., Manga, M., Rudolph, M., & Olson, P. (2016). Quantifying melt production and degassing rate at mid-ocean ridges from global mantle convection models with plate motion history. *Geochemistry, Geophysics, Geosystems*, *17*(7), 2884–2904.

Li, M., & McNamara, A. (2013). The difficulty for subducted oceanic crust to accumulate at the Earth's core-mantle boundary. *Journal of Geophysical Research*, *118*, 1807-1816.

Li, M., McNamara, A., & Garnero, E. (2014). Chemical complexity of hotspots caused by cycling oceanic crust through mantle reservoirs. *Nature Geoscience*, *7*(5), 366–370.

Li, Y., Deschamps, F., & Tackley, P. J. (2014). The stability and structure of primordial reservoirs in the lower mantle: insights from models of thermochemical convection in three-dimensional spherical geometry. *Geophysical Journal International*, *199*(2), 914–930.

Maljaars, J. M., Richardson, C. N., & Sime, N. (2020). LEoPart: a particle library for FEniCS. *Computers and Mathematics with Applications*. doi: 10.1016/j.camwa.2020.04.023

Manga, M. (1996). Mixing of heterogeneities in the mantle: effect of viscosity differences. *Geophysical Research Letters*, *23*(4), 403–406.

McNamara, A. K., & Zhong, S. (2004). Thermochemical structures within a spherical mantle: Superplumes or piles? *Journal of Geophysical Research*, *109*, B07402.

McNamara, A. K., & Zhong, S. (2005). Thermo–chemical structures beneath Africa and the Pacific Ocean. *Nature*, *437*, 1136–1139.

Morgan, H., & Scott, L. R. (2018). Towards a unified finite element method for the Stokes equations. *SIAM Journal on Scientific Computing*, *40*(1), A130–A141.

Mulyukova, E., Steinberger, B., Dabrowski, M., & Sobolev, S. V. (2015). Survival of LLSVPs for billions of years in a vigorously convecting mantle: replenishment and destruction of chemical anomaly. *Journal of Geophysical Research*, *120*(5), 3824–3847.

Nakagawa, T., Nakakuki, T., & Iwamori, H. (2015). Water circulation and global mantle dynamics: Insight from numerical modeling. *Geochemistry, Geophysics, Geosystems*, *16*(5), 1449–1464.

Nakagawa, T., & Tackley, P. (2004). Thermo-chemical structure in the mantle arising from a three-component convective system and implications for geochemistry. *Physics of the Earth and Planetary Interiors*, *146*(1-2), 125–138.

Nakagawa, T., & Tackley, P. (2008). Lateral variations in CMB heat flux and deep mantle seismic velocity caused by a thermal-chemical-phase boundary layer in 3D spherical convection. *Earth and Planetary Science Letters*, *271*, 348–358.

Nakagawa, T., Tackley, P., Deschamps, F., & Connolly, J. (2010). The influence of MORB and harzburgite composition on thermo-chemical mantle convection in a 3-D spherical shell with self-consistently calculated mineral physics. *Earth and Planetary Science Letters*, *296*, 403–412.

Nakagawa, T., & Tackley, P. J. (2014). Influence of combined primordial layering and recycled MORB on the coupled thermal evolution of Earth's mantle and core. *Geochemistry, Geophysics, Geosystems*, *15*(3), 619–633.

O'Farrell, K. A., & Lowman, J. P. (2010). Emulating the thermal structure of spherical shell convection in plane-layer geometry mantle convection models. *Physics of the*

Earth and Planetary Interiors, *182*(1-2), 73–84.

O'Farrell, K. A., Lowman, J. P., & Bunge, H.-P. (2013). Comparison of spherical-shell and plane-layer mantle convection thermal structure in viscously stratified models with mixed-mode heating: implications for the incorporation of temperature-dependent parameters. *Geophysical Journal International*, *192*(2), 456–472.

Ogawa, M. (2003). Chemical stratification in a two-dimensional convecting mantle with magmatism and moving plates. *Journal of Geophysical Research*, *108*, 2561.

Pietruszka, A. J., Norman, M. D., Garcia, M. O., Marske, J. P., & Burns, D. H. (2013). Chemical heterogeneity in the Hawaiian mantle plume from the alteration and dehydration of recycled oceanic crust. *Earth and Planetary Science Letters*, *361*, 298–309.

Ricolleau, A., Perrillat, J.-P., Fiquet, G., Daniel, I., Matas, J., Addadd, A., ... Guignot, N. (2010). Phase relations and equation of state of a natural MORB: Implications for the density profile of subduction oceanic crust in the Earth's lower mantle. *Journal of Geophysical Research*, *115*(B08202).

Ringwood, A. (1990). Phase transformations and differentiation in subducted lithosphere: Implications for mantle dynamics, basalt petrogenesis, and crustal evolution. *The Journal of Geology*, *90*, 611-643.

Ringwood, A., & Irifune, T. (1988). Nature of the 650-km seismic discontinuity: Implications for mantle dynamics and differentiation. *Nature*, *331*, 131–136.

Saal, A., Kurz, M., Hart, S., Blusztajn, J., Blichert-Toft, J., Liang, Y., & Geist, D. (2007). The role of lithospheric gabbros on the composition of Galapagos lavas. *Earth and Planetary Science Letters*, *257*(3-4), 391–406.

Schuberth, B. S. A., Bunge, H., Steinle-Neumann, G., Moder, C., & Oeser, J. (2009). Thermal versus elastic heterogeneity in high-resolution mantle circulation models with pyrolite composition: high plume excess temperatures in the lowermost mantle. *Geochemistry, Geophysics, Geosystems*, *10*(1), Q01W01.

Shorttle, O., & Maclennan, J. (2011). Compositional trends of icelandic basalts: Implications for short–length scale lithological heterogeneity in mantle plumes. *Geochemistry, Geophysics, Geosystems*, *12*, Q11008.

Sime, N. (2020). *GeoPart: Particles in geodynamics supporting code.* https://bitbucket.org/nate-sime/geopart.

Sime, N., Maljaars, J. M., Wilson, C. R., & van Keken, P. E. (submitted). An exactly mass conserving and pointwise divergence free velocity method: application to compositional buoyancy driven flow problems in geodynamics. *Submitted to Geochemistry, Geophysics, Geosystems*.

Sleep, N. H. (1988). Gradual entrainment of a chemical layer at the base of the mantle by overlying convection. *Geophysical Journal International*, *95*(3), 437–447.

Sobolev, A. V., Hofmann, A. W., Sobolev, S. V., & Nikogosian, I. K. (2005). An olivine-free mantle source of Hawaiian shield basalts. *Nature*, *434*(7033), 590–597.

Starkey, N. A., Stuart, F. M., Ellam, R. M., Fitton, J. G., Basu, S., & Larsen, L. M. (2009). Helium isotopes in early Iceland plume picrites: Constraints on the composition of high ^{3}He/^{4}He mantle. *Earth and Planetary Science Letters*, *277*(1-2), 91–100.

Stuart, F. M., Lass-Evans, S., Fitton, J. G., & Ellam, R. M. (2003). High ^{3}He/^{4}He ratios in picritic basalts from Baffin Island and the role of a mixed reservoir in mantle plumes. *Nature*, *424*(6944), 57–59.

Tackley, P. J. (2000). Mantle convection and plate tectonics: Toward an integrated physical and chemical theory. *Science*, *288*, 2002–2007.

Trompert, R., & Hansen, U. (1998). Mantle convection simulations with rheologies that generate plate-like behaviour. *Nature*, *395*(6703), 686–689.

Tsuchiya, T. (2011). Elasticity of subducted basaltic crust at the lower mantle pressures: Insights on the nature of deep mantle heterogeneity. *Physics of the Earth and Planetary Interiors*, *188*, 142–149.

Xie, S., & Tackley, P. J. (2004). Evolution of U-Pb and Sm-Nd systems in numerical models of mantle convection. *Journal of Geophysical Research*, *109*, B11204.

Yan, J., Ballmer, M. D., & Tackley, P. J. (2020). The evolution and distribution of recycled oceanic crust in the earth's mantle: Insight from geodynamic models. *Earth and Planetary Science Letters*, *537*, 116171.

Zindler, A., & Hart, S. (1986). Chemical geodynamics. *Annual Reviews of Earth Planetary Sciences*, *14*, 493–571. doi: 10.1146/annurev.ea.14.050186.002425